Inorganic Chemistry

Communication

pubs.acs.org/IC

Intercrystal Self-Assembly for the Design of High-Quality Nickel Molybdate Nanocrystals

Kenji Saito,* Shotaro Kazama, Yuki Sato, Tatsuto Yui, and Masayuki Yagi

Department of Materials Science and Technology, Faculty of Engineering, Niigata University, 8050 Ikarashi-2, Niigata 950-2181, Japan

Supporting Information

ABSTRACT: Nanowire of nickel molybdate hydrate, being recognized as an emerging supercapacitor material, was synthesized from the intercrystal self-assembly process (commonly referred to as oriented aggregation or attachment). The detailed lattice image of a $NiMoO_4 \cdot 0.75H_2O$ nanowire and the intermediate nanostructure before reaching the interplanar binding were successfully captured by means of high-resolution transmission and scanning electron microscopies. $NiMoO_4 \cdot 0.75H_2O$ possessed highly crystalline surface and internal nanostructures.

A solution-phase synthesis yields enough inorganic crystals for a wide spectrum of researches at relatively low cost.[1−3] Yet, crystallinity that exerts an influence on the device performance[4] depends mostly on experimental conditions (as represented by the synthesis temperature) especially under the template-free environment, forcing us to spend a lot of time and energy optimizing the conditions. A better way to prevent the undesirabilities includes producing a situation in which the primary particles grow larger by a specific mechanism, in order to reduce the likelihood of a loss in the crystallinity.

Oriented aggregation, known as a nonclassical pathway, is a crystal growth mechanism in which small crystals fuse with each other by intercrystal collision or attractive interactions in an appropriate distance.[5−7] Thus far, extensive efforts have been made to deeply understand the particular mechanism in metal and simple metal oxide and sulfide systems; however, the guiding principle in synthesizing a functional binary system remains inarticulated.

Thus far, we have reported on the synthesis of a functional binary oxide, *monoclinic* $Ag_2Mo_2O_7$ (m-$Ag_2Mo_2O_7$), with nanowire morphology.[8] In this case, the controlled dissolution rate of the Mo component, by changing the starting Mo compounds, under reflux determines the growth processes of the resulting crystals. MoO_3 that is less soluble in a solvent (water) leads to a sluggish nucleation of the primary particle on its surface, and the size homogeneity of the primary particles results in interplanar binding, forming secondary particles (oriented aggregation). On the other hand, a soluble Mo source, $(NH_4)_6Mo_7O_{24}$, forms primary particles of varied sizes with the reaction of Ag^+ immediately, leading to the classic Ostwald ripening. The crystallinities, as well as the photocatalytic performances, posed by the difference in the growth mechanisms had a striking difference (m-$Ag_2Mo_2O_7$ grown by the oriented aggregation possessed exceptional high crystallinity and showed activity for the photocatalytic O_2 evolution reaction). However, routine use as a means of the design of high-quality functional binary oxides requires expansion of the basic synthesis strategy to the other molybdate systems first.

Nickel molybdate hydrate ($NiMoO_4 \cdot nH_2O$) has been attracting much attention, for example, as an emerging supercapacitor material.[9] Most approaches employ hydrothermal methods being conducted at relatively higher temperatures and internal pressures. Herein, we synthesized the targeted material by reflux in order to slow down the nucleation process, as in the case of $Ag_2Mo_2O_7$, and to promote further growth via the oriented aggregation mechanism in the template- and additive-free environment. The material we target here is $NiMoO_4 \cdot 0.75H_2O$ because, unlike the common $NiMoO_4 \cdot nH_2O$ (PDF 13-0128), the detailed nanostructural and growth analyses of $NiMoO_4 \cdot 0.75H_2O$ have yet to be made.[10,11]

The powder precipitated from a homogeneous solution containing $(NH_4)_6Mo_7O_{24} \cdot 4H_2O$ and $Ni(NO_3)_2 \cdot 6H_2O$ after 1 day of reflux showed X-ray diffraction (XRD) patterns quite similar to those of $Co(MoO_4)(H_2O)_{0.75}$ (PDF 74-8729; Figure 1a). The resulting patterns have so far been well-examined by other groups, and the result from the Rietveld refinement derives that the chemical composition corresponds to $NiMoO_4 \cdot 0.75H_2O$.[10] Using a thermogravimetry−differential thermal analysis (TG−DTA), the water content of the reflux-synthesized nanowire was determined to be 0.89 (Figure S1), which nearly corresponds to the XRD result.

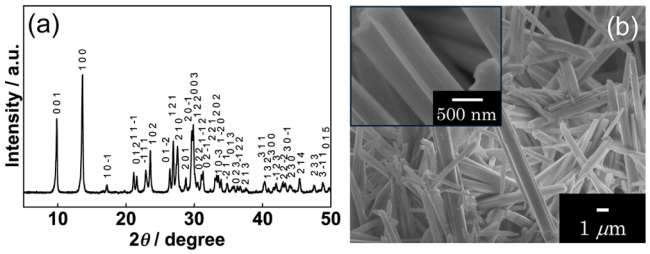

Figure 1. (a) XRD patterns and (b) FE-SEM image of $NiMoO_4 \cdot 0.75H_2O$. The inset shows the magnified view of part b.

The field-emission scanning electron microscopy (FE-SEM) image (Figure 1b) of $NiMoO_4 \cdot 0.75H_2O$ shows nanowires with a large diameter distribution (200−700 nm). Any structure other

Received: March 19, 2015
Published: September 2, 2015

DOI: 10.1021/acs.inorgchem.5b00625
Inorg. Chem. 2015, 54, 8869−8871

than the nanowire was not observed in the sample. In order to make certain of whether the crystallographic parameter of a single nanowire agrees with that previously refined using the Rietveld method (a = 6.7791 Å, b = 6.8900 Å, c = 9.2486 Å, α = 76.681°, β = 83.960°, and γ = 74.218°),[10] high-resolution transmission electron microscopy (HR-TEM) experiments were carried out. Figure 2a shows the image, in which the width of the

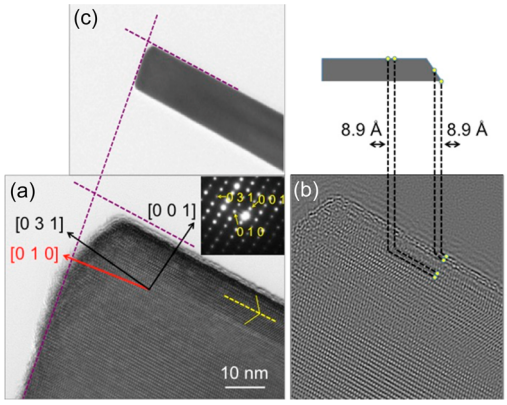

Figure 2. (a) HR-TEM image of a single $NiMoO_4 \cdot 0.75H_2O$ nanowire. The black and red arrows represent the direction derived from electron diffraction (a, inset). The yellow dashed lines indicate a twin boundary in the $NiMoO_4 \cdot 0.75H_2O$ lattice. (b) IFFT image of a portion of part a. (c) Lower-magnification image of part a. The purple dashed lines that are written across parts a and c are added in order to highlight the nanowire's profile. The supposable surface structure is displayed in the upper right corner.

fringes (8.9 Å) that exist throughout the single nanowire agreed with the d spacing of (001) of *triclinic* $NiMoO_4 \cdot 0.75H_2O$ (8.9 Å). Electron diffraction consists of a discrete crystal lattice of distinct spots, indicating a single-crystalline nature (inset of Figure 2a). At first blush, [031], which is nearly parallel to the longitudinal axis of the nanowire, seemed to correspond to the growth direction of the nanowire. However, the lower-magnification image (Figure 2c) showed a nanowire's tip evidently inclined from the perpendicular, with respect to the longitudinal axis of the nanowire. The same trend was observed in other nanowires. Thus, we think that [010] orthogonal to the inclined nanowire tip corresponds to the intrinsic growth direction of the nanowire.

The nanostructured surface consists of two- to three-atom-thick layers with a blurred, brighter contrast compared to the periodic internal structure (Figure 2a). We thus computed the inverse Fourier transform of the surface image using a fast Fourier transformation algorithm (IFFT), in order to visualize the surface structure more clearly (Figure 2b). As a result, the 8.9 Å lattice spacing of the surface nanostructure agreed with those of the internal bulk structure. Therefore, the nanowire surface is crystalline, and the reason why the contrast distinctly differs by location (surface vs inside) is because two to three surface atoms arrange, for example, in a comb manner, as shown in Figure 2 (top-right).

For the purpose of elucidating a growth mechanism of the $NiMoO_4 \cdot 0.75H_2O$ nanowire, we first examined a temporal evolution of the resulting powders (Figure 3). The recognizable particles are not observed even after a lapse of 5−7 h. We thus hourly sampled a portion of the reaction solutions and characterized the filtrate. This is based on the assumption that the resulting particles are the trace level and the consecutive sampling does not affect the solution concentration during

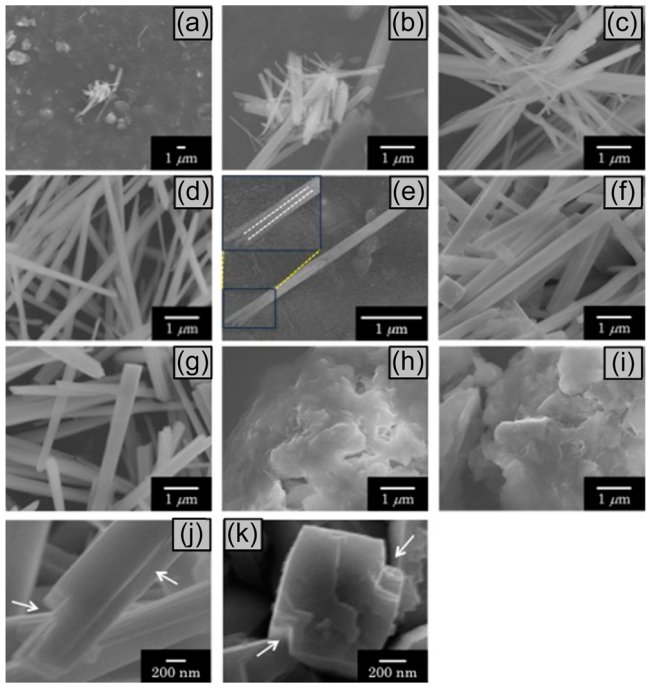

Figure 3. FE-SEM images regarding temporal evolution of the $NiMoO_4 \cdot 0.75H_2O$. These nanostructures are collected after (a) 1, (c) 2, (d) 3, (f) 5, and (g) 6 h of reflux of aqueous solutions containing $(NH_4)_6Mo_7O_{24} \cdot 4H_2O$ and $Ni(NO_3)_2 \cdot 6H_2O$. (b) Magnified view focused on the nanowire morphologies of part a. (e) Single nanostructure, half of which consists of a small nanowire bundle. The inset of part e is a magnified view of the branched nanowire's tip. The white dotted lines are added for clarity. The control experiments in which the separate aqueous solutions of (h) $(NH_4)_6Mo_7O_{24} \cdot 4H_2O$ and (i) $Ni(NO_3)_2 \cdot 6H_2O$ are refluxed for 1 h were conducted as well. (j and k) Imperfect final structures (24 h of reflux) lacking partial building blocks, which are marked with white arrowheads.

reaction. For the sampling, we attached a conductive C tape for FE-SEM measurements on a nonconductive membrane filter after standard filtration under reduced pressure. A tiny amount of residue embedded on the filter was corrected by peeling away the tape. The short (~1 μm) and thin (~60 nm) nanowires were visible in the first 1 h, besides formless particles with micrometer-scale (Figure 3a,b). The small nanowires tend to get long and thick as the reaction time increases. Most importantly, a single nanostructure was successfully detected before the interplanar binding was reached (half of the single nanostructure consists of a small nanowire bundle with 60−80 nm diameter, which is undetectable at the final form; Figure 3e). In contrast, the initially observed species, the formless particle, becomes difficult to observe as the reaction time increases, and it apparently disappears at last. The trend is associated with its role as a supply source of $NiMoO_4 \cdot 0.75H_2O$.[12] Actually, two separate $(NH_4)_6Mo_7O_{24} \cdot 4H_2O$ and $Ni(NO_3)_2 \cdot 6H_2O$ solutions under reflux both result in a tiny amount of precipitate even after 1 h of reflux, and the shape of the precipitate is similar to that of the targeted component (Figure 3a, upper left corner). As another important aspect, there existed a final structure having partial lack of building blocks (Figure 3j,k). Such imperfect structures are observable when particle growth proceeds via the self-assembly of crystals.[13] The imperfect final structures will be grown as a consequence of the slower diffusion of the nanocrystal than that of the molecule and cluster. The existence of a twin boundary of Figure 2a further supports particle growth by interplanar binding.

DOI: 10.1021/acs.inorgchem.5b00625
Inorg. Chem. 2015, 54, 8869−8871

The Brunauer–Emmett–Teller (BET) surface area of $NiMoO_4{\cdot}0.75H_2O$ was just 1 $m^2\ g^{-1}$, although it possesses a nanosized structure (Figure 1b). This value is an order of magnitude smaller than that of a hydrothermally synthesized $NiMoO_4{\cdot}0.75H_2O$ nanowire (31 $m^2\ g^{-1}$)[11] but is comparable to that of the m-$Ag_2Mo_2O_7$ nanowire (4 $m^2\ g^{-1}$), which was synthesized and grown in the same environment as this research (reflux synthesis and the oriented aggregation mechanism). The reflux-synthesized $NiMoO_4{\cdot}0.75H_2O$ and m-$Ag_2Mo_2O_7$ possess their own crystal structures; m-$Ag_2Mo_2O_7$ and $NiMoO_4{\cdot}0.75H_2O$ consist of 1D MoO_6 chains sharing those edges and corners and stepped MoO_4 dimers, respectively.[8,10] There is no particular factor, such as a supposable open pore, that is involved in counting of the BET surface areas. Meanwhile, a tangible similarity in the physical properties resides (their exceptional highly crystalline surfaces, as revealed by the HR-TEM results). Thus, a flattened surface nanostructure of $NiMoO_4{\cdot}0.75H_2O$ is considered to lead to the exceptionally low BET surface area, as is the case in m-$Ag_2Mo_2O_7$.

The preliminary pseudocapacitor performance of the $NiMoO_4{\cdot}0.75H_2O$ nanowire was assessed. The capacitance reaches 739 F g^{-1}, which is comparable to that of the $NiMoO_4{\cdot}H_2O$ nanowire (682 F g^{-1}) at a discharge current density of 0.5 A g^{-1},[14] whereas it largely drops to 402 F g^{-1} when the current density is increased to 1.0 A g^{-1}. The $NiMoO_4{\cdot}0.75H_2O$ nanowire will have a potential to store electric charges, and optimization as well as in-depth characterization are currently underway.

The $NiMoO_4{\bullet}{\cdot}0.75H_2O$ nanowire was dehydrated by 700 °C calcination to afford *monoclinic* $NiMoO_4$ (m-$NiMoO_4$). The dehydration process does not severely impact the local nanostructure, as recognized by the HR-TEM images (Figure S2).

In summary, a *triclinic* $NiMoO_4{\cdot}0.75H_2O$ nanowire was synthesized by refluxing an aqueous solution of $(NH_4)_6Mo_7O_{24}{\cdot}4H_2O$ and $Ni(NO_3)_2{\cdot}6H_2O$. Using high-resolution electron microscopy techniques, the nanowire was found to grow in a direction along [010] and the particle growth was revealed to proceed by intercrystal self-assembly. The nanowire possessed an exceptionally low BET surface area and originated from the highly crystalline surface. $NiMoO_4{\cdot}0.75H_2O$ will have the potential to store electric charges. The dehydrated $NiMoO_4$ maintained the nanowire structure.

■ ASSOCIATED CONTENT

Supporting Information

The Supporting Information is available free of charge on the ACS Publications website at DOI: 10.1021/acs.inorgchem.5b00625.

Experimental section, a plot of TG–DTA, a HR-TEM image, and electron diffraction of the *m*-$NiMoO_4$ nanowire (PDF)

■ AUTHOR INFORMATION

Corresponding Author

*E-mail: ksaito@eng.niigata-u.ac.jp.

Notes

The authors declare no competing financial interest.

■ ACKNOWLEDGMENTS

K.S. acknowledges financial support of a Grant-in-Aid for Young Scientists B (Grant 26790012) from the Ministry of Education, Culture, Sports, Science and Technology (MEXT) of Japan, the Kurata Memorial Hitachi Science and Technology Foundation, and the Uchida Energy Science Foundation.

■ REFERENCES

(1) Murray, C. B.; Kagan, C. R.; Bawendi, M. G. *Annu. Rev. Mater. Sci.* **2000**, *30*, 545–610.
(2) Cushing, B. L.; Kolesnichenko, V. L.; O'Connor, C. J. *Chem. Rev.* **2004**, *104*, 3893–3946.
(3) Talapin, D. V.; Lee, J.-S.; Kovalenko, M. V.; Shevchenko, E. V. *Chem. Rev.* **2010**, *110*, 389–458.
(4) Shankar, K.; Basham, J. I.; Allam, N. K.; Varghese, O. K.; Mor, G. K.; Feng, X.; Paulose, M.; Seabold, J. A.; Choi, K.-S.; Grimes, C. A. *J. Phys. Chem. C* **2009**, *113*, 6327–6359.
(5) Bahrig, L.; Hickey, S. G.; Eychmüller, A. *CrystEngComm* **2014**, *16*, 9408–9424.
(6) Penn, R. L.; Banfield, J. F. *Science* **1998**, *281*, 969–971.
(7) Penn, R. L.; Soltis, J. A. *CrystEngComm* **2014**, *16*, 1409–1418.
(8) Saito, K.; Kazama, S.; Matsubara, K.; Yui, T.; Yagi, M. *Inorg. Chem.* **2013**, *52*, 8297–8299.
(9) Hu, X.; Zhang, W.; Liu, X.; Mei, Y.; Huang, Y. *Chem. Soc. Rev.* **2015**, DOI: 10.1039/C4CS00350K.
(10) Eda, K.; Kato, Y.; Ohshiro, Y.; Sugitani, T.; Whittingham, M. S. *J. Solid State Chem.* **2010**, *183*, 1334–1339.
(11) Ding, Y.; Wan, Y.; Min, Y.-L.; Zhang, W.; Yu, S.-H. *Inorg. Chem.* **2008**, *47*, 7813–7823.
(12) Biedunkiewicz, A.; Krawczyk, M.; Gabriel-Polrolniczak, U.; Figiel, P. *J. Therm. Anal. Calorim.* **2014**, *116*, 715–726.
(13) Zheng, X.-J.; Kuang, Q.; Xu, T.; Jiang, Z.-Y.; Zhang, S.-H.; Xie, Z.-X.; Huang, R.-B.; Zheng, L.-S. *J. Phys. Chem. C* **2007**, *111*, 4499–4502.
(14) Wan, H.; Jiang, J.; Ji, X.; Miao, L.; Zhang, L.; Xu, K.; Chen, H.; Ruan, Y. *Mater. Lett.* **2013**, *108*, 164–167.

DOI: 10.1021/acs.inorgchem.5b00625
Inorg. Chem. 2015, 54, 8869–8871